ISSN 1674-1056
http://cpb.iphy.ac.cn
http://iopscience.iop.org/cpb
中国物理 B
Chinese Physics
中国物理 Chinese Physics B

Solar energy full-spectrum perfect absorption and efficient photo-thermal generation

Zhefu Liao(廖喆夫), Zhengqi Liu(刘正奇), Qizhao Wu(吴起兆), Xiaoshan Liu(刘晓山), Xuefeng Zhan(詹学峰), Gaorong Zeng(曾高荣), and Guiqiang Liu(刘桂强)

Citation: Chin. Phys. B, 2021, 30 (**8**): 084206. DOI: 10.1088/1674-1056/ac0696
Journal homepage: http://cpb.iphy.ac.cn; http://iopscience.iop.org/cpb

What follows is a list of articles you may be interested in

Omnidirectional and compact Tamm phonon-polaritons enhanced mid-infrared absorber

Xiaomin Hua(花小敏), Gaige Zheng(郑改革), Fenglin Xian(咸冯林), Dongdong Xu(徐董董), and Shengyao Wang(王升耀)

Chin. Phys. B, 2021, 30 (**8**): 084202. DOI: 10.1088/1674-1056/abe22b

Broadband absorption enhancement with ultrathin MoS_2 film in the visible regime

Jun Wu(吴俊)

Chin. Phys. B, 2021, 30 (**2**): 024208. DOI: 10.1088/1674-1056/abc3b5

Actively tunable polarization-sensitive multiband absorber based on graphene

Ai-Li Cao(曹爱利), Kun Zhang(张昆), Jia-Rui Zhang(张佳瑞), Yan Liu(刘燕), and Wei-Jin Kong(孔伟金)

Chin. Phys. B, 2020, 29 (**11**): 114205. DOI: 10.1088/1674-1056/abb663

Ultra wide sensing range plasmonic refractive index sensor based on nano-array with rhombus particles

Jiankai Zhu(朱剑凯), Xiangxian Wang(王向贤), Xiaoxiong Wu(吴枭雄), Yingwen Su(苏盈文), Yueqi Xu(徐月奇), Yunping Qi(祁云平), Liping Zhang(张丽萍), and Hua Yang(杨华)$

Chin. Phys. B, 2020, 29 (**11**): 114204. DOI: 10.1088/1674-1056/abb229

Broadband visible light absorber based on ultrathin semiconductor nanostructures

Lin-Jin Huang(黄林锦), Jia-Qi Li(李嘉麒), Man-Yi Lu(卢漫仪), Yan-Quan Chen(陈彦权), Hong-Ji Zhu(朱宏基), Hai-Ying Liu(刘海英)

Chin. Phys. B, 2020, 29 (**1**): 014201. DOI: 10.1088/1674-1056/ab5787

Solar energy full-spectrum perfect absorption and efficient photo-thermal generation*

Zhefu Liao(廖喆夫), Zhengqi Liu(刘正奇)†, Qizhao Wu(吴起兆), Xiaoshan Liu(刘晓山), Xuefeng Zhan(詹学峰), Gaorong Zeng(曾高荣), and Guiqiang Liu(刘桂强)‡

College of Physics and Communication Electronics, Jiangxi Normal University, Nanchang 330022, China

(Received 8 May 2021; revised manuscript received 25 May 2021; accepted manuscript online 29 May 2021)

Designing and manufacturing cost-effective absorbers that can cover the full-spectrum of solar irradiation is still critically important for solar harvesting. Utilizing control of the lightwave reflection and transmission, metamaterials realize high absorption over a relatively wide bandwidth. Here, a truncated circular cone metasurface (TCCM) composed of alternating multiple layers of titanium (Ti) and silicon dioxide (SiO_2) is presented. Enabled by the synergetic of surface plasmon resonances and Fabry–Pérot resonances, the TCCM simultaneously achieves high absorptivity (exceed 90%), and absorption broadband covers almost the entire solar irradiation spectrum. In addition, the novel absorber exhibits great photo-thermal property. By exploiting the ultrahigh melting point of Ti and SiO_2, high-efficiency solar irradiation absorption and heat release have been achieved at 700 °C when the solar concentration ratio is 500 (*i.e.*, incident light intensity at 5×10^5 W/m^2). It is worth noting that the photo-thermal efficiency is almost unchanged when the incident angle increases from 0° to 45°. The outstanding capacity for solar harvesting and light-to-heat reported in this paper suggests that TCCM has great potential in photothermal therapies, solar desalination, and radiative cooling, *etc*.

Keywords: solar energy, photo-thermal generation, perfect absorption, plasmonic

PACS: 42.25.Bs, 42.60.Da, 73.40.Rw, 78.67.Pt **DOI:** 10.1088/1674-1056/ac0696

1. Introduction

As the development of the economy and the population continues to grow, energy has become a strategic issue for global sustainable development. Due to the abundant, non-polluting, and renewable characteristics of solar energy resources, the solar energy industry is growing rapidly. So far this year, solar energy has accounted for only 1% of renewable energy consumption. Recently, various photovoltaic (PV) devices have emerged continually, which can convert solar energy directly into electricity based on the photovoltaic effect. However, limited by the Shockley–Queisser limit, traditional single-junction PV devices can only use the restricted proportion of the solar spectrum.[1] Although a mass of work has been made to break the limit, such as multi-junction solar cells, these PV devices remain confronted with some dilemmas including high cost and complicated manufacturing processes. In order to exploit the solar spectrum as much as possible and exceed the Shockley–Queisser limit, the solar thermal system, which uses solar energy to heat absorber and raise the temperature, has given rise to tremendous attention over decades.[2]

For solar thermal applications,[3] the greatest challenge is how to realize high-efficiency solar energy harvesting. Therefore, the ultra-broadband absorbers, which play a pivotal role in solar thermal systems, have been the focus of solar energy research in recent years. Conventional absorbers are hardly to achieve high absorption and wide bandwidths while maintaining a small size. Luckily, the advent of metamaterial along with the rapid development of nanofabrication technologies has ameliorated this situation,[4–6] including perfect absorption[7–10] and meta-lens.[11] The metal–dielectric–metal (MIM) is the most typical structure of metamaterial absorbers.[12–21] Li *et al.* designed a periodic square ring nanostructure with high absorptivity composed of three layers.[22] The SiO_2 dielectric layer separated by titanium nitride (TiN) substrate layer and TiN square ring. Benefiting from the extremely high melting point of TiN and SiO_2, the absorber has no change in absorption spectral after annealing at 800 °C for 8 h and exhibits great thermal stability. It is worth noting that the operating temperature often exceeds 600 °C in high-temperature solar photo-thermal applications. Regrettably, the relatively narrow absorption bandwidth heavily impedes the practical application of this absorber, which only covers the visible region (400 nm–800 nm). In addition to using the same resonator, employing several different size resonators as a periodic unit is also a viable approach. Based on their previous single and dual-band absorber, Liu and co-workers computationally designed a system consisting of 16 sublattices, each sublattice containing a various size cross resonator.[23] In the system, the absorption spectrum can be accurately tailored by adjusting the permutation of differ-

*Project supported by the National Natural Science Foundation of China (Grant Nos. 11804134 and 11464019) and the Natural Science Foundation of Jiangxi Province, China (Grant No. 20202BBEL53036).

†Corresponding author. E-mail: zliu@jxnu.edu.cn

‡Corresponding author. E-mail: liugq@jxnu.edu.cn

© 2021 Chinese Physical Society and IOP Publishing Ltd

ent size cross resonators. Furthermore, the way of stacking multiple individual resonators along perpendicular direction comes into the picture while the limited transverse space is depleted. The incident lights of different wavelengths captured by various size resonators in a unit cell are the typical characteristic of this type of absorber. For instance, Cui *et al*. ingeniously designed a sawtooth-like anisotropic ultra-broadband metamaterial absorber with over 95% absorption in a range from 3 μm to 5.5 μm.[24] The position of the incident light trapped by the sawteeth structure gradually shifts downward as the wavelength increases. This study provides a new idea for the development of designing ultra-broadband absorbers. Not only limited to solar irradiation capture but the high temperature created by the photothermal effect also cannot be ignored. With introduction of refractory materials in recent years, the thermal stability of absorber has been greatly improved. Refractory materials generally possess high melting points and have been proven to have broadband losses due to their large imaginary dielectric constants.[25] The absorbers made of refractory and its composites perform well in terms of absorption performance and heat stability.

In this paper, we theoretically design a truncated circular cone metasurface absorber and numerically simulate the spectral response. A novel multiple resonator structure integrates the advantages of high photothermal conversion efficiency and low-cost, which is capable of utilizing the full spectrum of solar energy. The mechanism of strong absorption can be attributed to the synergistic effect of surface plasmon resonances and Fabry–Pérot resonances via analyzing the electric field intensity distributions at different wavelengths. For photo-thermal generation, the transient-state and steady-state temperature distributions are also calculated in various incident light intensities. In addition, we find the absorber is insensitive to incident angle. These superior performances provide the absorber with great potential in solar photo-thermal applications.

2. Structure and theory method

The ultra-broadband metamaterial absorber covering the entire solar irradiation spectrum proposed by us is shown in Fig. 1, which is made up of two parts, including a truncated circular cone structure and a relatively thick metal substrate. The truncated circular cone structure composed of alternating SiO_2/Ti layers, and the thickness of each SiO_2 layer (h_1) and Ti layer (h_2) is 100 nm and 20 nm, respectively. The total number of alternating SiO_2/Ti layer pairs (N) is 7. In addition, θ represents the angle between generatrix and horizontal plane. r and p are the bottom radius of cone structure and lattice constant. The dielectric spacer is SiO_2 with the thickness of 70 nm (h_3). The thickness of Ti substrate (h_4) is set as 200 nm, which is larger than the skin depth of solar irradiation in Ti. Thus, it is thick enough to prevent light transmission. The dielectric constants of SiO_2 and Ti are taken from Palik's book.[26] Besides, due to the relatively small thermo-optical coefficient and the ultra-high melting point of Ti and SiO_2, the absorber offers fine thermal stability.[27] In terms of experimental preparation, magnetron sputtering and electron beam lithography can be used to fabricate the proposed metamaterial absorber.

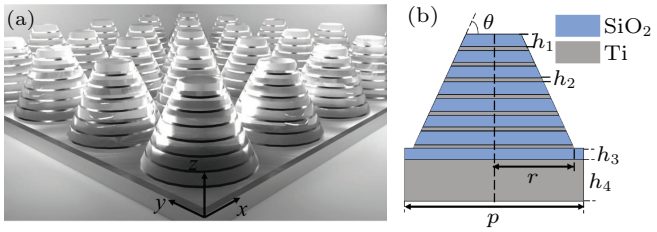


Fig. 1. (a) Schematic diagram of an array of TCCM absorbers. (b) Corresponding cross-section view of TCCM with component materials and geometric parameters.

To calculate the spectral response of absorber, absorptivity ($A(\lambda)$) based on the Poynting theorem can be expressed as

$$A(\lambda) = 1 - R(\lambda) - T(\lambda), \tag{1}$$

where $R(\lambda)$ and $T(\lambda)$ represent reflectivity and transmissivity, respectively. Due to the opaqueness of the substrate, the transmissivity of incident light can be completely neglected (*i.e.*, $A(\lambda) = 1 - R(\lambda)$). The solar spectral absorption efficiency α can be calculated by the following equation:

$$\alpha = \frac{\int_{280}^{4000} A(\lambda) I_{\mathrm{AM1.5}}(\lambda)\,\mathrm{d}\lambda}{\int_{280}^{4000} I_{\mathrm{AM1.5}}(\lambda)\,\mathrm{d}\lambda}, \tag{2}$$

where the $I_{\mathrm{AM1.5}}(\lambda)$ is the spectral intensity of solar irradiation at the Air Mass 1.5 Global.

On the side, the thermal energy diffusion between the absorber or component of the absorber and the surrounding medium is also taken into account during the incident light on and off. In order to investigate the transient-state temperature distribution of the absorber during heat transfer under continuous waves (CW), we must consider the multiple-layers absorber as many components.[28] Each component is applied to following equation:[28,29]

$$C_{\mathrm{p}}\rho\frac{\partial T}{\partial t} + \nabla\cdot(-k\nabla T) = q_0, \tag{3}$$

where C_{p}, ρ, and k are the specific heat capacity, mass density, and thermal conductivity coefficient of each material, respectively. T represents the temperature and is both time- and space-dependent. q_0 is heat source per unit volume. But, in our case, q_0 is equivalent to resistive heat (Q_{d}) generated by light absorption. The Q_{d} is given by

$$Q_{\mathrm{d}} = \frac{1}{2}\varepsilon_0\omega\,\mathrm{Im}(\varepsilon_{\mathrm{r}})\,|E|^2, \tag{4}$$

where ε_0 and ε_{r} are permittivity of vacuum and relative permittivity of material, and ω is the angular frequency of incident

light. $|\boldsymbol{E}|$ is the magnitude of the electric field. The thermal diffusion equation (Eq. (3)) reduces to Eq. (5), while the temperature field reaches steady-state (*i.e.*, the temperature of the absorber and surrounding medium under incident light does not change over time). Thus, equation (5) can be concisely written as

$$\nabla \cdot (-k\nabla T) = q_0. \tag{5}$$

3. Results and discussion

Figure 2(a) depicts the comparison among absorption, reflection, and transmission of TCCM absorber under normal CW, and the wavelength covers from 280 nm to 6000 nm. Benefiting from the 200-nm opaque Ti substrate, the transmission of incident light can be overlooked. Clearly, the absorption spectra hold high-level absorption from ultraviolet to mid-infrared range. Especially in the range of 348 nm to 4190 nm, the average absorption rate is over 90%, suggesting the bandwidth of absorption reaches 3842 nm. Although an absorption dip appears at near 4000 nm due to the impedance mismatch with free space, the absorption spectrum still covers almost the whole spectrum of solar irradiation.[30] These typical characteristics including high absorption efficiency and wide bandwidth have significant advantages over other absorbers.[31–34] Based on the $I_{\text{abs}} = A(\lambda)I_{\text{AM1.5}}(\lambda)$, the absorption curve of the TCCM absorber under the AM 1.5 Global is plotted in Fig. 2(b).

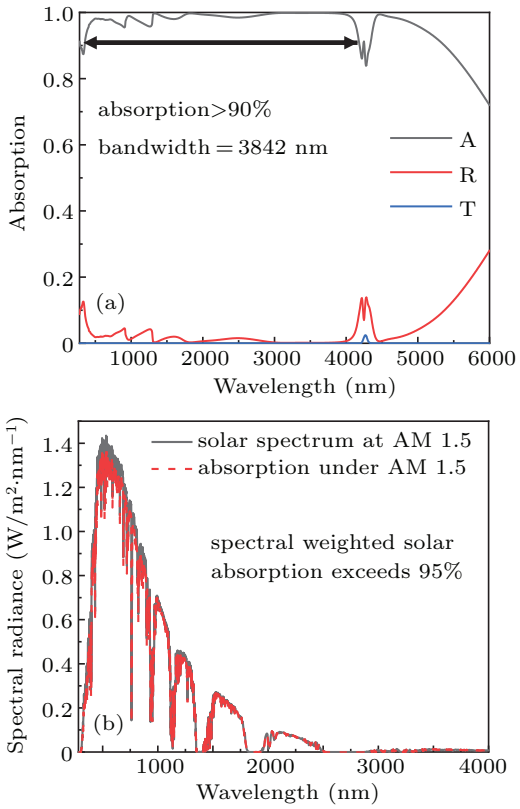


Fig. 2. (a) Optical properties of the TCCM absorber under normal illumination range from 280 nm to 6000 nm. (b) The standard spectrum of solar radiance AM 1.5 Global (solid line) and the solar energy absorption of the TCCM absorber under the AM 1.5 Global (dashed line).

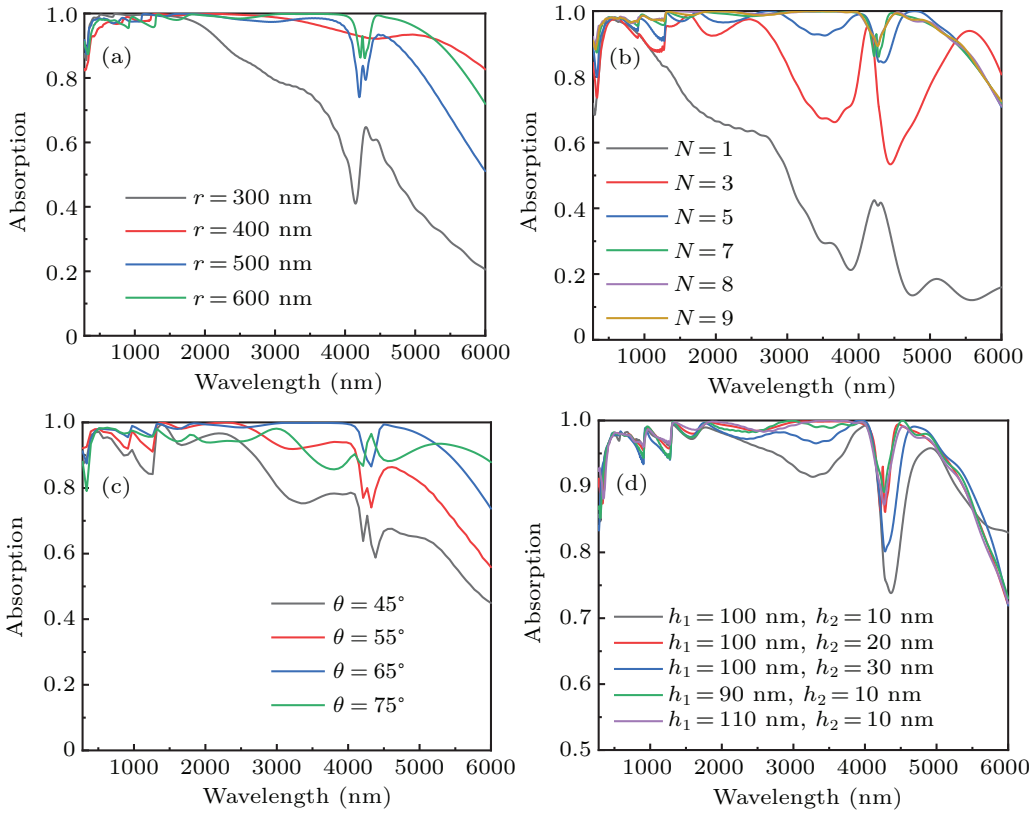


Fig. 3. The absorption spectrum of different geometric parameters. (a) The absorption of TCCM with bottom radius (r) of cone structure increasing from 300 nm to 600 nm and other parameters are fixed. (b) The absorption spectra of TCCM with increasing of the total number of pair (N). (c) The absorption of TCCM with the angle (θ) between generatrix and horizontal plane changing from 45° to 75° and other parameters are fixed. (d) The absorption of TCCM with different thickness combinations of SiO_2 layer (h_1) and Ti layer (h_2).

There is an extremely high degree of overlap between the solar irradiation spectrum under AM 1.5 Global and the absorption spectrum, indicating the TCCM absorber possesses a great capacity of solar spectral absorption efficiency. As it turned out, the solar spectral weighted absorption efficiency α is calculated as 95% based on Eq. (2). Such high solar spectral absorption efficiency can be attributed to the full spectrum absorption, unlike previously reported absorbers that can only cover visible and near-infrared.

The geometrical parameters of the nanostructure, which affect the absorption of the TCCM absorber, are shown in Fig. 3, such as the bottom radius (r) of cone structure and the angle (θ) between generatrix and horizontal plane. It is obvious that the absorption spectra improve clearly in the mid-infrared band with r increases, and the visible and near-infrared band is nearly unaffected. At last, the entire absorption spectrum maintains near-perfect absorption. Meanwhile, as N increases, the absorption gradually grows in the infrared region, but the increment decreases significantly, and eventually the absorption efficiency approaches saturation (Fig. 3(b)). For these phenomenons, we can conclude there is a strong correlation between the wavelength of the plasmonic resonance peak and the size of resonator. Moreover, as the resonator size increases, the wavelength is red-shifted. As shown in Fig. 3(c), the changing trend of the absorption spectrum is nonlinear with θ increases. Initially, the absorption is improved as the angle increases from 45°, and the absorption reaches optimum while $\theta = 65°$. However, with a further increase in θ, the absorption spectrum was inhibited. It is can be explained by the fact that metabolic angle θ causes the size of all resonators in a period change, which further makes the whole absorption spectrum change. For the effect of the thickness of SiO_2 layer and Ti layer on the absorption efficiency, as shown in Fig. 3(d), $h_1 = 100$ nm and $h_2 = 20$ nm is optimal which makes the nanostructure size as large as possible.

In order to further investigate the physical mechanism behind the ultra-broadband near-perfect absorption phenomenon, we analyzed the electric field distribution of TCCM at several wavelengths. In the following simulations, geometric parameters are default values unless otherwise specified. We can easily observe multiple surface plasmon resonances are excited in the incident light, and the position of resonances is shifting gradually from top to bottom with the wavelengths increase from 377 nm to 5120 nm, as shown in Figs. 4(a)–4(d). It is certainly supports the above inference that the wavelength of the plasmonic resonance peak is positively correlated with resonator size. Apparently, at $\lambda = 1000$ nm, adjacent Ti layers reflect incident light back and forth in the SiO_2 layer, playing the role of Fabry–Pérot interferometer. In addition, since the thickness of Ti-layer and SiO_2-layer is smaller than the incident light wavelength, the effective medium theory can be applied to explain the TCCM absorber and treat the whole nanostructure as a homogeneous material with anisotropic permittivities.[35] For this nanostructure, the permittivity $\varepsilon_\perp$ parallels to the optical axis have a negative real part and a nonzero imaginary part, opposite to the permittivity $\varepsilon_{||}$ perpendicular to the optical axis, indicating that it is a typical hyperbolic metamaterial and has excellent light field modulation performance.[36,37] Moreover, compared to other multilayer absorbers with infinite extension in the y direction, such as sawtooth anisotropic metamaterial slab[24] and refractory prismoid absorber,[38] the TCCM absorber has excellent polarization-independence due to its symmetric structure, which is of great practical application.

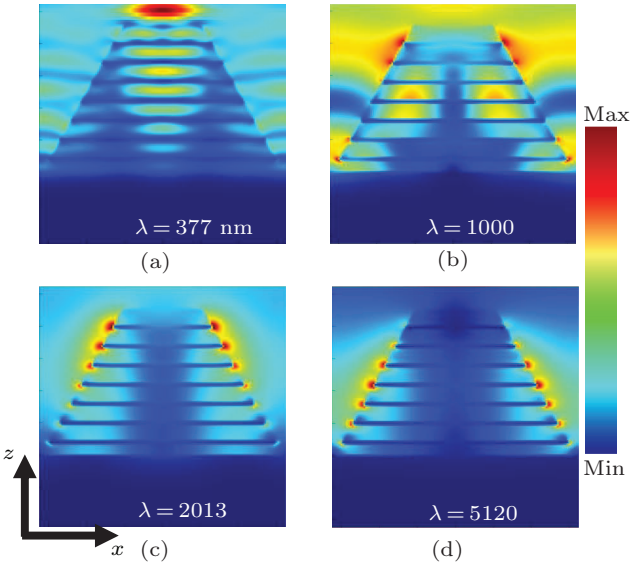


Fig. 4. (a)–(d) The normalized electric field distribution at 377 nm, 1000 nm, 2013 nm, and 5120 nm, respectively.

The temperature variation for TCCM absorber under incident light is discussed by simulating the photo-thermal generation and thermal diffusion. Therefore, we divide the heating process into two parts: the heat generated by the multiple plasmon resonance and the heat exchange between the absorber and surrounding medium. It is well known that the flux of solar irradiation with AM1.5 Global is 1000 W/m^2. In this work, we define C as the solar concentration (*i.e.*, $1C = 1000$ W/m^2). In order to facilitate comparison of results, the initial room temperature is set as 22 °C, and used in the following simulations. For transient-state, the temperature distribution of TCCM absorber and surrounding medium can be solved by time-dependent heat equation (Eq. (3)). In fact, the surrounding medium dominates the magnitude of the transient time scale, as the heat transfer process is very rapid in the absorber. Thus, significant temperature differences can only be obtained at very short times and high excitation intensities.[39] Figure 5(a) shows the distribution of heat power volume density Q_d (*i.e.*, power absorption density) with the incident illumination of 1000-nm wavelength, and the major of the heat

power distributes in the interface between metal and dielectric. Furthermore, the thermal effect of the individual absorber is studied to obtain the performance of the entire array in the medium. The temperature map with obvious temperature diversities can be obtained until the C increases to 10^6 at an ultrashort time of 10 ns, as shown in Fig. 5(b). As excepted, the hotspots in distribution of the heat power volume density (Fig. 5(a)) and the temperature map (Fig. 5(b)) have a great deal of similarity. As shown in Fig. 5(c), the result of the temperature difference map showed that the maximum temperature difference is risen to 105 °C. In particular, it should be noted that the duration of the illumination is only 26 ns, which indicates that the proposed structure has great potential for ultrafast photothermal applications.

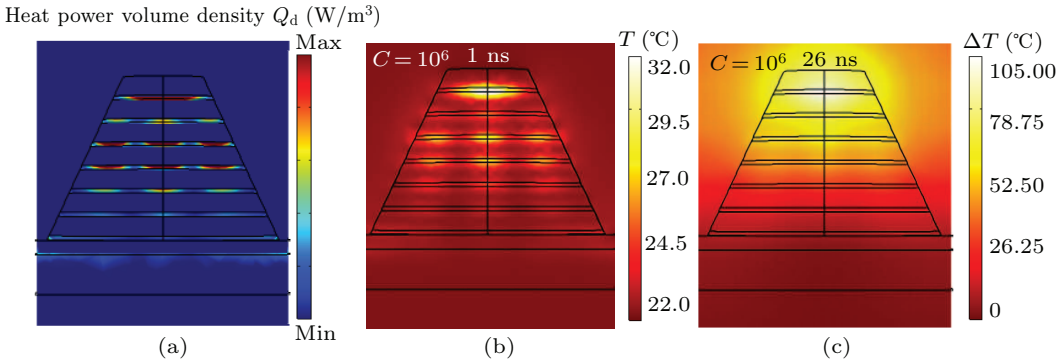


Fig. 5. (a) Heat power volume density distribution of TCCM under plane wave illumination of 1000-nm wavelength. (b)–(c) The temperature distribution of TCCM when $C = 10^6$ at 1 ns and 26 ns, respectively.

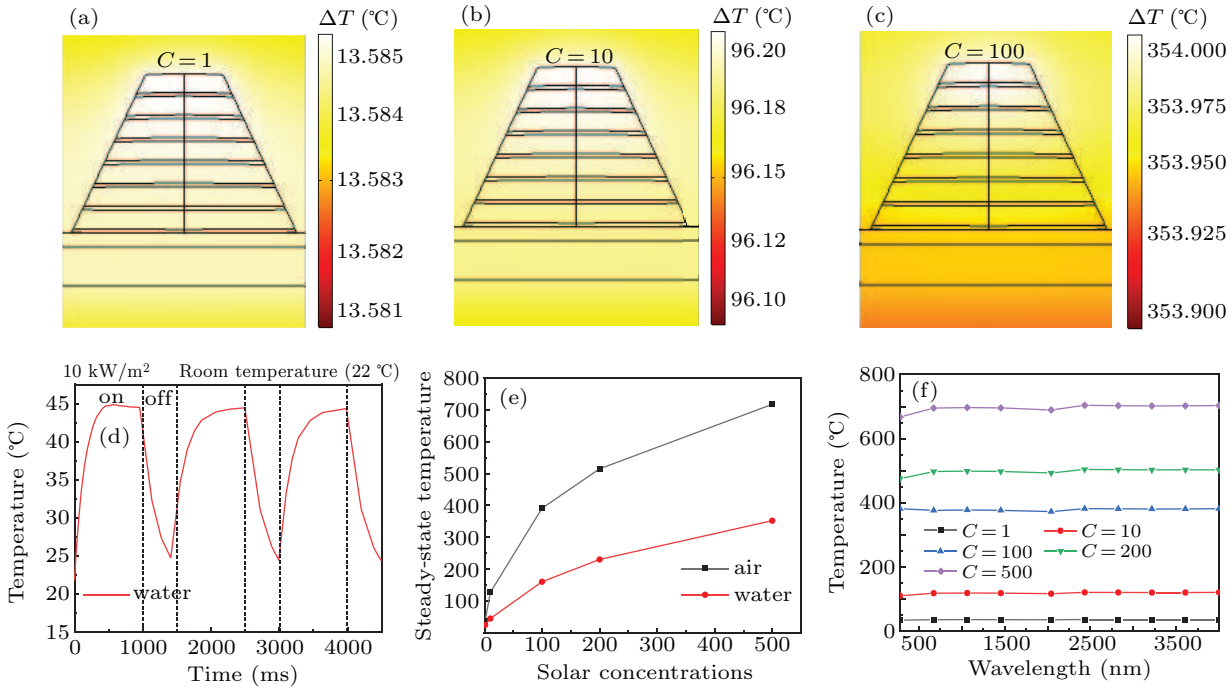


Fig. 6. (a)–(c) Steady-state temperature difference distributions of the TCCM absorber in air for solar concentrations of $C = 1$, $C = 10$, and $C = 100$, respectively. (d) Temperature of TCCM absorber in water as a function of time under on/off modulated light with solar concentration of $C = 10$. (e) The steady-state temperature of TCCM absorber in air or water with various solar concentrations. (f) The steady-state temperature of TCCM absorber under incident light of different wavelengths for $C = 1$, 10, 100, 200, and 500, respectively.

Furthermore, we calculate and plot the steady-state temperature difference distribution for TCCM with several solar concentrations and different wavelengths. In terms of application, the solar concentration C can be flexibly adjusted according to the actual demand by using the concentrator reasonably, generally around 10–1000.[40] In Fig. 6(a), both the TCCM absorber and surrounding environment reach steady-state while $C = 1$. The temperature distribution is uniform and the maximum temperature difference exceeds 13 °C. Combined with the high absorption properties of TCCM in the near-infrared, it has demonstrated its ability to be applied to plasmonic photothermal therapy.[41] In addition, by covering with polyethylene bubble wrapfilm to reduce the convective losses, the average temperature can be further increased.[42] While the solar concentration increases to 10 and 100, respectively, the maximum temperature difference (ΔT) increases to 96.20 °C and

354 °C accordingly, as shown in Figs. 6(b)–6(c). We also simulate the temperature rise/fall with on/off modulated light in Fig. 6(d). The temperature reaches a maximum of 45 °C after about 1000 ms, and then cools to room temperature after 500 ms, when the medium is water and $C = 1$. Figure 6(e) plots the steady-state temperature as a function of solar concentration. Although being in water with a higher specific heat capacity and thermal conductivity causes a significant drop in temperature compared to being in air (717.30 °C), the maximum temperature still reaches 351.76 °C when $C = 500$ under 1000-nm incident light. As shown in Fig. 6(f), regardless of solar concentration, the temperature fluctuation of TCCM at different wavelengths is very small, which means that TCCM can be excited by light in the ultraviolet to mid-infrared range to achieve the same photo-thermal performance. This result proves beyond doubt that TCCM absorber is not limited to applications in the field of solar energy.

In practical application, the sun irradiation is not always perpendicular to the absorber, so an incident-angle insensitive absorber is coveted. As shown in Fig. 7(a), the absorption curve at oblique incidence is somewhat different from that at vertical incidence (Fig. 2(a)), but the same high-level absorption is still maintained. This indicates that the proposed absorber is angle-insensitive in its spectral response. For photothermal, compared to vertical incidence (Fig. 5(b)), the temperature is even higher in 45° incidence reaching 36.45 °C. Similarly, the steady-state temperature at oblique incidence reaches 369.51 °C (Fig. 7(c)) higher than at vertical incidence (Fig. 6(c)). Overall, these findings demonstrate that the TCCM absorber is incident-angle insensitive both in terms of spectral response and photothermal effects.

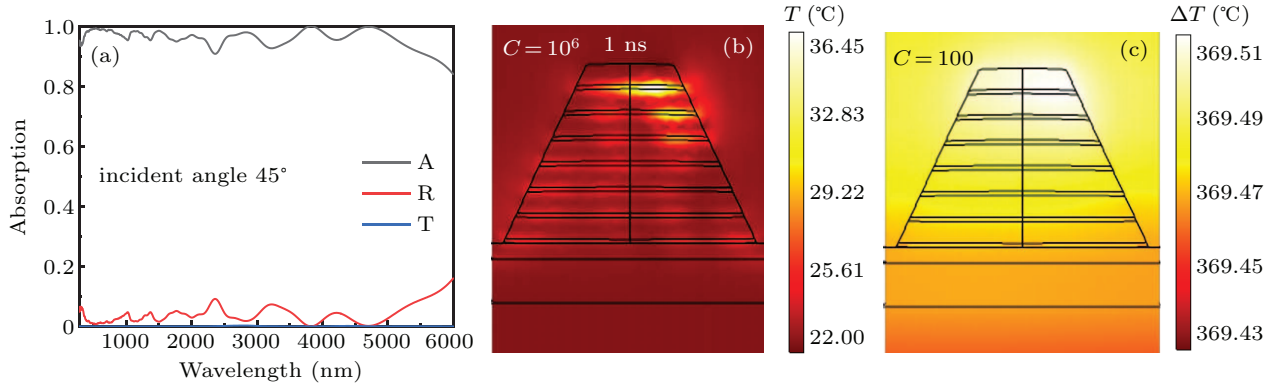


Fig. 7. (a) Optical properties of the TCCM absorber with incident angle of 45°. (b) Transient-state temperature distribution under incident angle of 45° at 1 ns, with solar concentration at C= 10^6. (c) Steady-state temperature difference distribution at an incident angle of 45° and solar concentration of $C = 100$.

4. Conclusions

In conclusion, we have built the computational model to simulate the optical response of the truncated circular cone metasurface absorber, whose high absorption broadband (348 nm–4190 nm) almost covers the whole solar irradiation spectrum. The solar spectral weighted absorption efficiency reaches 95%. The effect of geometrical parameters on the absorption performance and physical mechanism was also investigated. More importantly, using numerical methods, we studied the transient-state and steady-state temperature distributions at different incident light wavelengths and solar concentration. The maximum temperature reaches 717.30 °C when the solar concentration is 500. At various wavelengths, the structure shows outstanding performance stability both in terms of spectral response and photothermal effect. In addition, the nanostructure exhibits incident-angle insensitivity. These excellent properties make the proposed absorber can be wide application in solar energy solar and plasmonic photothermal therapy.

References

[1] Shin D, Kang G, Gupta P, Behera S, Lee H, Urbas A M, Park W and Kim K 2018 *Adv. Opt. Mater.* **6** 1800317
[2] Khodasevych I E, Wang L, Mitchell A and Rosengarten G 2015 *Adv. Opt. Mater.* **3** 852
[3] Jia Y, Ren P and Fan C 2020 *Chin. Phys. B* **29** 104210
[4] Su V C, Chu C H, Sun G and Tsai D P 2018 *Opt. Express* **26** 13148
[5] Wu Q N, Lan F, Tang X P and Yang Z Q 2015 *Chin. Phys. Lett.* **32** 107801
[6] Yang J, Luo F, Kao T S, Li X, Ho G W, Teng J, Luo X and Hong M 2014 *Light: Sci. Appl.* **3** 185
[7] Zhou L, Tan Y, Wang J, Xu W, Yuan Y, Cai W, Zhu S and Zhu J 2016 *Nat. Photon.* **10** 393
[8] Qin F, Chen X, Yi Z, Yao W, Yang H, Tang Y, Yi Y, Li H and Yi Y 2020 *Sol. Energy Mater. Sol. Cells* **211** 110535
[9] Zhu Y, Tang B, Yang N, Lang X, Su J and Li Z 2021 *Physica E* **126** 114449
[10] Zhu Y, Tang B and Jiang C 2019 *Appl. Phys. Express* **12** 032009
[11] Chen M K, Chu C H, Lin R J, Chen J W, Huang Y T, Huang T T, Kuo H Y and Tsai D P 2019 *Jpn. J. Appl. Phys.* **58** SK0801
[12] Fu W, Han Y, Li J, Wang H, Li H, Han K, Shen X and Cui T 2016 *J. Phys. D: Appl. Phys.* **49** 285110
[13] Kim Y J, Yoo Y J, Kim K W, Rhee J Y, Kim Y H and Lee Y 2015 *Opt. Express* **23** 3861
[14] Chen Y, Li X, Luo X, Maier S A and Hong M 2015 *Photon. Res.* **3** 54
[15] Huang Y, Liu L, Pu M, Li X, Ma X and Luo X 2018 *Nanoscale* **10** 8298
[16] Huang L J, Li J Q, Lu M Y, Chen Y Q, Zhu H J and Liu H Y 2020 *Chin. Phys. B* **29** 014201

[17] Wang B X, Huang W Q and Wang L L 2017 *RSC Adv.* **7** 42956
[18] Cao A L, Zhang K, Zhang J R, Liu Y and Kong W J 2020 *Chin. Phys. B* **29** 114205
[19] Ren Y, Zhou T, Jiang C and Tang B 2021 *Opt. Express* **29** 7666
[20] Tang B, Yang N, Huang L, Su J and Jiang C 2020 *IEEE Photon. J.* **12** 1
[21] Shi J X, Zhang W C, Xu W, Zhu Q, Jiang X, Li D D, Yan C C and Zhang D H 2015 *Chin. Phys. Lett.* **32** 094204
[22] Li W, Guler U, Kinsey N, Naik G V, Boltasseva A, Guan J, Shalaev V M and Kildishev V 2014 *Adv. Mater.* **26** 7959
[23] Liu X, Tyler T, Starr T, Starr A F, Jokerst N M and Padilla W J 2011 *Phys. Rev. Lett.* **107** 045901
[24] Cui Y, Fung K H, Xu J, Ma H, Jin Y, He S and Fang N X 2012 *Nano Lett.* **12** 1443
[25] Doiron B, Mota M, Wells M P, Bower R, Mihai A, Li Y, Cohen L F, Alford N M, Petrov P K, Oulton R F and Maier S A 2019 *ACS Photon.* **6** 240
[26] Palik E D 1985 *Handbook of Optical Constants of Solids* (Boston: Academic Press) p. 189
[27] Komma J, Schwarz C, Hofmann G, Heinert D and Nawrodt R 2012 *Appl. Phys. Lett.* **101** 041905
[28] Pustovalov V K 2016 *RSC Adv.* **6** 81266
[29] Chen X, Chen Y, Yan M and Qiu M 2012 *ACS Nano* **6** 2550
[30] Tittl A, Harats M G, Walter R, Yin X, Schaäferling M, Liu N, Rapaport R and Giessen H 2014 *ACS Nano* **8** 10885
[31] Hao J, Wang J, Liu X, Padilla W J, Zhou L and Qiu M 2010 *Appl. Phys. Lett.* **96** 251104
[32] Wang Z, Zhang Z M, Quan X and Cheng P 2018 *Sol. Energy* **159** 329
[33] Putnin T, Lertvachirapaiboon C, Ishikawa R, Shinbo K, Kato K, Ekgasit S, Ounnunkad K and Baba A 2019 *Opto-Electron. Adv.* **2** 190010
[34] Zhang D and Sugioka K 2019 *Opto-Electron. Adv.* **2** 190002
[35] Wood B, Pendry J B and Tsai D P 2006 *Phys. Rev. B* **74** 115116
[36] Bohren C F and Huffman D R 1998 *Absorption and Scattering of Light by Small Particles* (Weinheim: Wiley-VCH)
[37] Zhang Z, Liang Y and Xu T 2017 *Opto-Electron. Eng.* **44** 276
[38] Liu Z, Zhong H, Liu G, Liu X, Wang Y and Wang J 2020 *Opt. Express* **28** 31763
[39] Chen M, He Y, Wang X and Hu Y 2018 *Sol. Energy* **161** 17
[40] Li P, Liu B, Ni Y, Liew K K, Sze J, Chen S and Shen S 2015 *Adv. Mater.* **27** 4585
[41] Manrique-Bedoya S, Abdul-Moqueet M, Lopez P, Gray T, Disiena M, Locker A, Kwee S, Tang L, Hood R L, Feng Y and Large N 2020 *J. Phys. Chem. C* **124** 17172
[42] Li Y, Lin C, Wu Z, Chen Z, Chi C, Cao F, Mei D, Yan H, Tso C Y, Chao C Y and Huang B 2021 *Adv. Mater.* **33** 2005074